NAT'L INST. OF STAND & TECH
A11107 049241

NIST
PUBLICATIONS

NIST Technical Note 1529

Carbon-Loaded Polymer Composites Used as Human Phantoms: Theoretical Models for Predicting Low-Frequency Dielectric Behavior

Richard G. Geyer
James R. Baker-Jarvis
Michael D. Janezic
Raian K.F. Kaiser

QC
100
U5753
#1529
2003
c.2

NIST
nal Institute of Standards and Technology
logy Administration, U.S. Department of Commerce

NIST Technical Note 1529

Carbon-Loaded Polymer Composites Used as Human Phantoms: Theoretical Models for Predicting Low-Frequency Dielectric Behavior

Richard G. Geyer
James R. Baker-Jarvis
Michael D. Janezic
Raian K.F. Kaiser

Radio-Frequency Technology Division
Electronics and Electrical Engineering Laboratory
National Institute of Standards and Technology
325 Broadway
Boulder, Colorado 80305

June 2003

U.S. Department of Commerce
Donald L. Evans, Secretary

Technology Administration
Phillip J. Bond, Under Secretary of Commerce for Technology

National Institute of Standards and Technology
Arden L. Bement, Jr., Director

Certain commercial entities, equipment, or materials may be identified in this document in order to describe an experimental procedure or concept adequately. Such identification is not intended to imply recommendation or endorsement by the National Institute of Standards and Technology, nor is it intended to imply that the entities, materials, or equipment are necessarily the best available for the purpose.

National Institute of Standards and Technology Technical Note 1529
Natl. Inst. Stand. Technol. Tech. Note 1529, 43 pages (June 2003)
CODEN: NTNOEF

U.S. GOVERNMENT PRINTING OFFICE
WASHINGTON: 2003

For sale by the Superintendent of Documents, U.S. Government Printing Office
Internet: bookstore.gpo.gov Phone: (202) 512-1800 Fax: (202) 512-2250
Mail: Stop SSOP, Washington, DC 20402-0001

Contents

1 **Introduction** 2

2 **Lorentz-Lorenz, Clausius-Mossotti, Maxwell-Garnett, and Bruggeman Effective Medium Formulations** 6
- 2.1 Lorentz-Lorenz and Clausius-Mossotti Relations 6
- 2.2 Maxwell-Garnett and Bruggeman Relations 9
- 2.3 Modified Clausius-Mossotti Relation for Penetrable or Nonpenetrable Dispersed Particles 10

3 **Effective-Medium Formulations with Local Particle Aggregates** 14
- 3.1 Clausius-Mossotti Adaptation to Aggregate Model 14
- 3.2 Bruggeman Adaptation to Aggregate Model 16
- 3.3 Maxwell-Garnett Adaptation to Aggregate Model 17

4 **Measurements and Theory** 21

5 **Conductivity Temperature Dependence of Carbon-Black-Filled Polymers** 27
- 5.1 General Effect of Temperature Changes 27
- 5.2 Variable-Temperature Measurements on Carbon- Black Conductive Polymers 32

6 **Summary** 35

7 **References** 37

Carbon-Loaded Polymer Composites Used as Human Phantoms: Theoretical Models for Predicting Low-Frequency Dielectric Behavior

Richard G. Geyer, James R. Baker-Jarvis, Michael D. Janezic
Raian K.F. Kaiser

National Institute of Standards and Technology
Radio-Frequency Technology Division
Boulder, CO 80305

Conductive polymers loaded with carbon black are considered for use as semisolid biologic phantom materials. Adapted forms of Clausius-Mossoti, Maxwell-Garnett, and Bruggeman predictive dielectric mixing rules are considered that take into account disordered cluster topologies of the conductive particles in a dielectric composite. The disordered cluster suspensions can lead to rapid, nonlinear increases of permittivity and conductivity at volume-loading fractions far below the close-packing limit, where the percolation threshold would normally be approached in well- stirred metal-dielectric composites.

The measured low-frequency electrical properties of fabricated carbon-black-loaded silicone composites exhibit a threshold percolation at carbon loading fractions of one-third the close-packing limit. This conductivity and permittivity behavior is predicted by an adapted form of the classical Bruggeman rule that takes into account the cluster topology of the carbon black particles in the fabricated composites.

Conductivity measurements of carbon-black-loaded silicone polymer composites from 10 to 25 °C exhibit a temperature behavior similar to that of an extrinsic, partially compensated n-type semiconductor. The measured conductivity dependence with temperature can be related to the conduction-band density of states, as well as donor and acceptor concentrations in the composite. A large positive temperature coefficient with respect to resistance was observed at temperatures greater than 40 °C for the 7 % by weight carbon black-loaded silicone composite, which is consistent with nonpercolative behavior at these temperatures.

Key words: Carbon-loaded polymer; conductivity; dielectric; disordered suspensions; effective medium; mixing rules; nano- composite; percolation; permittivity; phantom

Chapter 1

Introduction

The development of materials that simulate the relevant electromagnetic properties of the human body is crucial to studies of low-frequency electromagnetic interaction with the body, as well as health effects of microwaves and interaction of wireless transmitters with human tissue [1]. When such materials are used as phantoms, standardized methods for evaluating and assessing the interaction of personal medical electronic devices (PMEDs) and metal weapons with magnetic fields generated by hand-held (HH) and walk-through (WT) metal detectors can also be developed and improved. A review of various phantom materials previously developed for use at low RF frequencies has been given by Baker-Jarvis, Kaiser, Janezic, Paulter, and Stricklett [1]. Some of these phantom materials are based on liquids and salts or various gelling agents and salts. Dielectric liquids generally work well at low frequencies because mobile ions from the salts can mimic the dielectric loss characteristics of human tissue. Examples of low-frequency conductivity data for various human tissues are shown in Fig. 1.1.

Semisolid materials, however, have several advantages over liquids in that they allow test objects to be permanently embedded or encapsulated at particular positions. The use of semi-solid phantom materials that simulate the electromagnetic properties of the human body over the frequency range at which metal detectors operate allows standardized testing for HH and WT metal sensors designed for detecting metal objects concealed within human body cavities.

One semisolid composite that can potentially be used for phantom materials is a carbon-black-loaded polymer. Carbon black is commonly chosen for its electrical conductivity and low cost, and the electrical conductivity of a polymer can be greatly adjusted and improved by incorporating carbon-black powders. Understanding the mechanisms of conduction and electromagnetic-wave propagation is critical to the development of these composite materials in phantoms that simulate the human body. A complicating factor generally not taken into account in predictive dielectric mixing

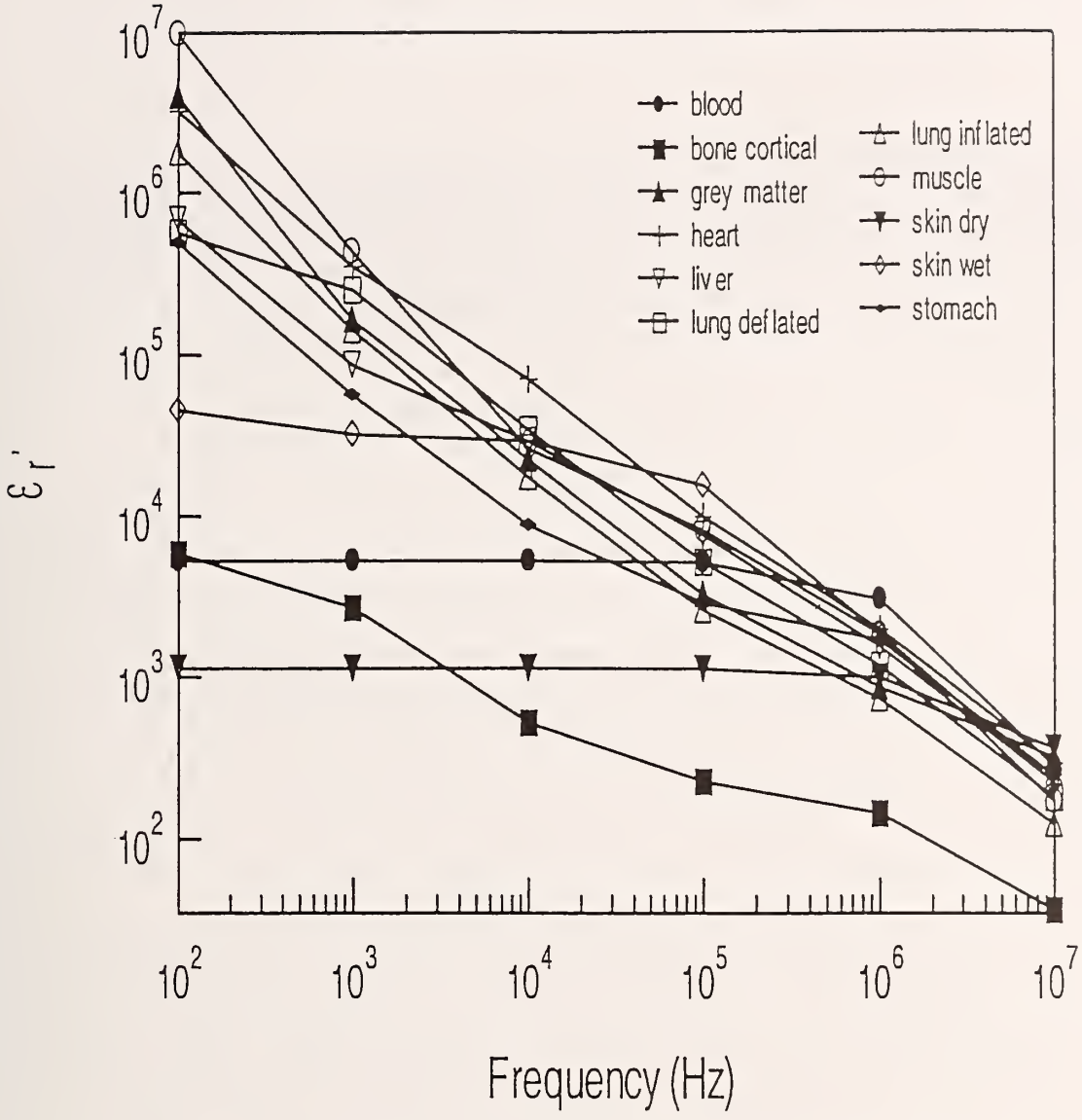

Figure 1.1: Measurements of conductivity of various body tissues as function of frequency. After Gabriel et al. [2] (no uncertainties assigned).

rules [3] is that carbon black may also form conducting clusters that depend on the total loading. The existence of carbon-black clusters affects the threshold level at which percolation occurs. A knowledge of how the volume fraction of the clusters depends on the carbon-black loading in the polymer and how, in turn, the electric properties of the composite phantom material depend on the topological structure of the clusters is important. The development of appropriate electromagnetic models that account for connective clustering of conductive inclusions in a dielectric medium permits predictive understanding of the electrical properties of carbon black-loaded polymers and optimizes the fabrication process of acceptable phantom composite materials.

In general, the effective electrical properties of an inhomogeneous medium that is composed of particles of one substance embedded in a continuum of a different material is a complicated function of the permittivities and conductivities of the constituents, the particle shape and size distributions, the volume loading, and the spatial arrangement of the distributions. The loading constituent may take the form of small spheres, ellipsoids, platelets, rods, or other shapes. The bulk properties of the composite will also depend on the alignment of the loading particles and therefore may be dielectrically or magnetically anisotropic. In addition, the bulk properties of the composite will generally not be a symmetric function of the volume-fraction of the matrix and filler. When any of these parameters have nonzero variance, the predictive theoretical problem becomes very difficult to solve. Permittivities and conductivities of disordered suspensions are difficult to handle, even when the suspended particles are spheres with a uniform size distribution.

If the composite medium is electrically isotropic in nature, the well-known Clausius-Mossotti approximation may be utilized, provided that only dipole interactions are present. For regular particle array suspensions, the assumption of dipole interactions is usually valid only in the limiting case of low volumetric loading. Higher multipole interactions between the loading particles become more important when the particles approach contact, so that the Clausius-Mossotti approximation breaks down under higher volumetric loading conditions. When there are random or disordered distributions, higher multipole interactions can occur with any volumetric loading and must be considered. These higher-order multipole interactions depend inversely on increasing powers of the interparticle distance and can often be observed as a strong nonlinear dependence of the effective permittivity or conductivity when plotted as a function of the volumetric filling factor.

In this report we review the general effective permittivities predicted by the theoretical models of Clausius-Mossotti, Lorentz-Lorenz, Maxwell-Garnett, and Bruggeman, highlighting some of their fundamental differences. We then consider the adaptation of the Clausius-Mossotti, Bruggeman, and Maxwell-Garnett rules to effective media in which the particle-size distribution has negligible variance, but in which aggregates or local clusters can form where local contact exists between the loading particles. These

models have application to conductive carbon particle and insulating polymer composites, which are currently being tested for use in human phantoms. Lastly, we compare the adapted aggregate forms of the Clausius-Mossotti, Bruggeman, and Maxwell-Garnet theoretical effective permittivity predictions with room-temperature laboratory dielectric data obtained on carbon-silicone composites.

Chapter 2

Lorentz-Lorenz, Clausius-Mossotti, Maxwell-Garnett, and Bruggeman Effective Medium Formulations

2.1 Lorentz-Lorenz and Clausius-Mossotti Relations

The Lorentz-Lorenz relation [4-6] is given by

$$\frac{\epsilon'_{eff} - 1}{\epsilon'_{eff} + 2} = \beta = \frac{4}{3}\pi N\alpha, \tag{2.1}$$

which relates the effective permittivity ϵ'_{eff} and the polarization β of a spherical sample of the medium to the number density N of a suspension of point dipoles, and the polarizability α of each dipole. The Lorentz-Lorenz relation was essentially developed to describe point polarizable dipole particles embedded in vacuum. If the polarization of a spherical sample of the medium expressed by eq (2.1) is equated to the volume filling factor ν of a distribution of metal spheres having individual isolated polarizabilities $\alpha = R^3$, eq (2.1) reduces to the Clausius-Mossotti relation,

$$\frac{\epsilon'_{eff} - 1}{\epsilon'_{eff} + 2} = \beta = \frac{4}{3}\pi N\alpha = \nu. \tag{2.2}$$

Equation (2.2) relates the polarization β to the *in situ* dipole polarizability α and dipole number density, which is related to the macroscopic permittivity of a spherical sample.

If α includes the effects of all higher-order multipole interactions, eq (2.2) could be used to calculate the *exact* permittivity. However, this has seldom been accomplished for atomic or molecular dipoles, since so few higher-order atomic multipole polarizabilities are known. We see that the well-known Lorentz "catastrophe" occurs when the number density is such that $4\pi N\alpha/3 = 1$, for which a singularity in permittivity occurs, where permittivity rapidly increases. Similarly, the Clausius-Mossotti relation erroneously predicts that there is a permittivity singularity when $\nu = 1$. However, equal-sized spheres can never meet this condition nor can they completely fill space. Generally, the Lorentz catastrophe is prevented by a conductive transition which occurs when any collection of conducting spheres begin to touch each other. The maximum packing density of a suspension of spheres of equal size depends upon their spatial arrangement. For cubic lattices the maximum possible volume filling factors ν_c are 0.52, 0.68, and 0.74, for sc, bcc, and fcc lattices, respectively. For random packing of equal-sized spheres, the maximum possible volume filling factor is $\nu_c = 0.63$ [7,8].

All regular or random or disordered distributions undergo a conductive transition when spherical loading particles make contact. In disordered carbon suspensions in a silicone matrix, we usually have no detailed control over interparticle carbon spacings. In this case, disordered samples contain local conductive regions (particle aggregates or clusters) where the critical loading density has been reached, and other nonconductive or dielectric regions with lower particle densities. At any filling factor below the critical value, a disordered system acts like a mixture of dielectric regions and conductive particle aggregates. Suspensions of dispersed particles both with no aggregates or clusters forming and with clusters forming are shown in Figures 2.1 and 2.2. With increasing volume-filling factors, the conductive aggregates grow at the expense of the dielectric regions. Hence, in contrast with the behavior or regular arrays of ordered suspensions, conduction in disordered suspensions occurs at different times in different regions of the sample and the dielectric anomaly is spread over an entire range of filling factors below ν_c. A critical filling factor still occurs at ν_c, though, when the entire suspension exhibits a polarization anomaly. The Clausius-Mossotti equation for a suspension of spheres of two constituents is given by

$$\frac{\epsilon'_{eff} - 1}{\epsilon'_{eff} + 2} = \nu_1 \frac{\epsilon'_1 - 1}{\epsilon'_1 + 2} + \nu_2 \frac{\epsilon'_2 - 1}{\epsilon'_2 + 2}, \tag{2.3}$$

where $\epsilon'_{eff} = \epsilon_{eff}/\epsilon_0$, $\epsilon'_1 = \epsilon_1/\epsilon_0$, and $\epsilon'_2 = \epsilon_2/\epsilon_0$ are, respectively, the relative permittivities of the suspension and the two particle types with respect to the permittivity ϵ_0 of free space (8.854×10^{-12} F/m); the volume fractions of the two particles are given by ν_1 and ν_2.

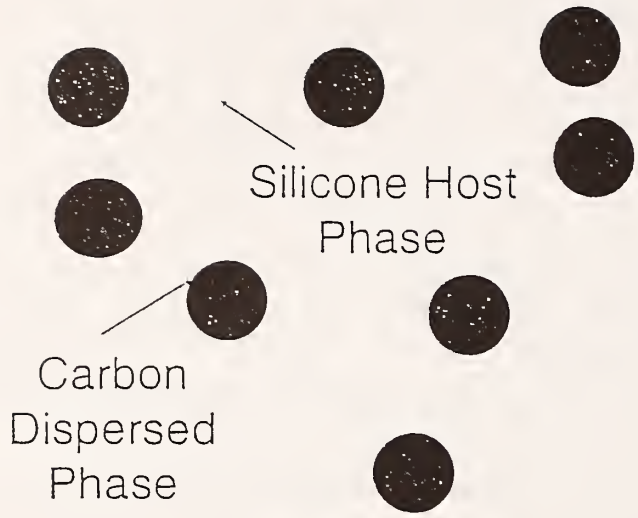

Figure 2.1: Disordered suspension of carbon particles in a silicone matrix host phase where no aggregates of the carbon particles exist.

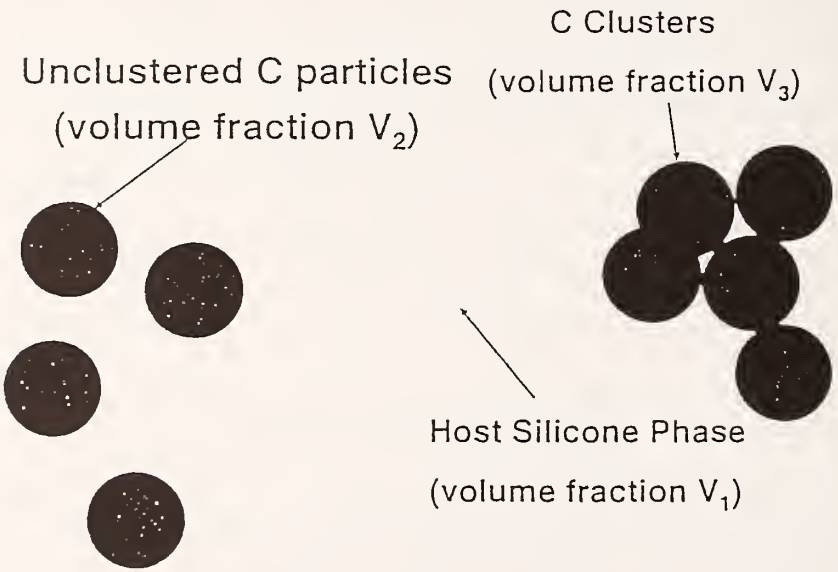

Figure 2.2: Disordered suspension of carbon particles in a silicone matrix where aggregates of the carbon particles exist.

2.2 Maxwell-Garnett and Bruggeman Relations

The Maxwell-Garnett effective medium approximation differs from the Clausius-Mossotti relation in that the inclusions are in a matrix background other than vacuum. For a two-phase composite, the Maxwell-Garnett approximation is given by [9],

$$\frac{\epsilon'_{eff} - \epsilon'_m}{\epsilon'_{eff} + 2\epsilon'_m} = \nu_1 \frac{\epsilon'_1 - \epsilon'_m}{\epsilon'_1 + 2\epsilon'_m}, \tag{2.4}$$

where $\epsilon'_m = \epsilon_m/\epsilon_0$ is the relative permittivity of the matrix (host), ϵ'_1 is the relative permittivity of the dispersed phase, and ν_1 is the volume fraction of the dispersed phase. The Maxwell-Garnett rule works fairly well if the dispersed phase inclusions make up a small fraction of the total volume. Note that the Maxwell-Garnett rule is not symmetric; that is, different effective permittivities are obtained when the roles of the matrix host and particle inclusions are interchanged, even if the volume fractions remain the same. We may write the effective permittivity of the composite for this topology as

$$\epsilon'_{eff} = \frac{\epsilon'_m [\epsilon'_1(1 + 2\nu_1) + 2\epsilon'_m(1 - \nu_1)]}{\epsilon'_1(1 - \nu_1) + \epsilon'_m(2 + \nu_1)}. \tag{2.5}$$

The Maxwell-Garnett dielectric mixing rule requires that

- the sizes of dispersed particles are much smaller than both the electromagnetic wavelength and the skin depth within the particle material,
- a *dilute* suspension of spherical (carbon) particles in a continuous host matrix (silicone).

Where there is significant aggregation or clustering of carbon particles, especially for dense composites, the Maxwell-Garnett model, although convenient, becomes inappropriate.

The Clausius-Mossotti approximation cannot be employed for mixtures of two constituents when the topology of the composite consists of an intermingling of many small, irregularly shaped regions having different complex permittivities. In this case, Bruggeman [10] proposed making the properties of the matrix or host the same as the effective medium itself and derived the following two-phase composite effective medium formulation for spherical elements,

$$V_1 \frac{\epsilon'_1 - \epsilon'_{eff}}{\epsilon'_1 + 2\epsilon'_{eff}} + V_2 \frac{\epsilon'_2 - \epsilon'_{eff}}{\epsilon'_2 + 2\epsilon'_{eff}} = 0, \tag{2.6}$$

where V_1 and V_2 are, respectively, the volume fractions occupied by phases of media 1 and 2. The Bruggeman model is a symmetric formulation, and the solution for the

effective permittivity for a two-phase composite leads to the solution of the following quadratic,

$$\epsilon_1'\epsilon_2' + [\epsilon_1'(2V_1 - V_2) + \epsilon_2'(2V_2 - V_1)]\,\epsilon_{eff}' - 2(\epsilon_{eff}')^2 \;=\; 0. \tag{2.7}$$

Implicit to the Bruggeman topological model [10] is that

- the suspended inclusions are distributed randomly;
- all suspended inclusions are very small compared with the size of the composite (and very large compared with atomic sizes);
- inclusions of the same type (material, size, form) are present in very large numbers and phases are very close together with negligible interstices;
- the composite consists of homogeneous and isotropic elements of two materials; and
- no embedding of one phase within the other is allowed.

One limitation of the Bruggeman formulation, as presently posed, is that it cannot be applied to a monodisperse suspension of spherical elements because such a suspension cannot fill all sample space, even for closest-packing densities.

The Lorentz-Lorenz, Maxwell-Garnett, and Bruggeman topological models are special cases of an n-phase mixture rule of the form

$$\frac{\epsilon_{eff}' - \epsilon_m'}{\epsilon_{eff}' + 2\epsilon_m'} = \nu_1 \frac{\epsilon_1' - \epsilon_m'}{\epsilon_1' + 2\epsilon_m'} + \nu_2 \frac{\epsilon_2' - \epsilon_m'}{\epsilon_2' + 2\epsilon_m'} + \cdots + \nu_n \frac{\epsilon_n' - \epsilon_m'}{\epsilon_n' + 2\epsilon_m'}, \tag{2.8}$$

where $\epsilon_{eff}', \epsilon_m'$ represent the relative permittivities for the effective medium and host medium, and $\epsilon_1', \epsilon_2', \cdots, \epsilon_n'$ represent the permittivities for suspended inclusions of types $1, 2, \cdots, n$. The factors $\nu_1, \nu_2, \cdots, \nu_n$ denote the respective volume fractions of inclusions $1, 2, \cdots, n$. The spherical inclusion geometry, which has minimum dipole moment and depolarization, are common to the Lorentz-Lorenz, Maxwell-Garnett, and Bruggeman models.

2.3 Modified Clausius-Mossotti Relation for Penetrable or Nonpenetrable Dispersed Particles

A modified Clausius-Mossotti derivation is given in [9,11], in which spherical dispersed particles of radius a, having arbitrary complex permittivity $\epsilon_p^* = \epsilon_p'(1 - \tan\delta_{e,p})$, and magnetic permeability $\mu_p' = \mu_p'(1 - \tan\delta_{m,p})$, are distributed on a uniform cubic lattice

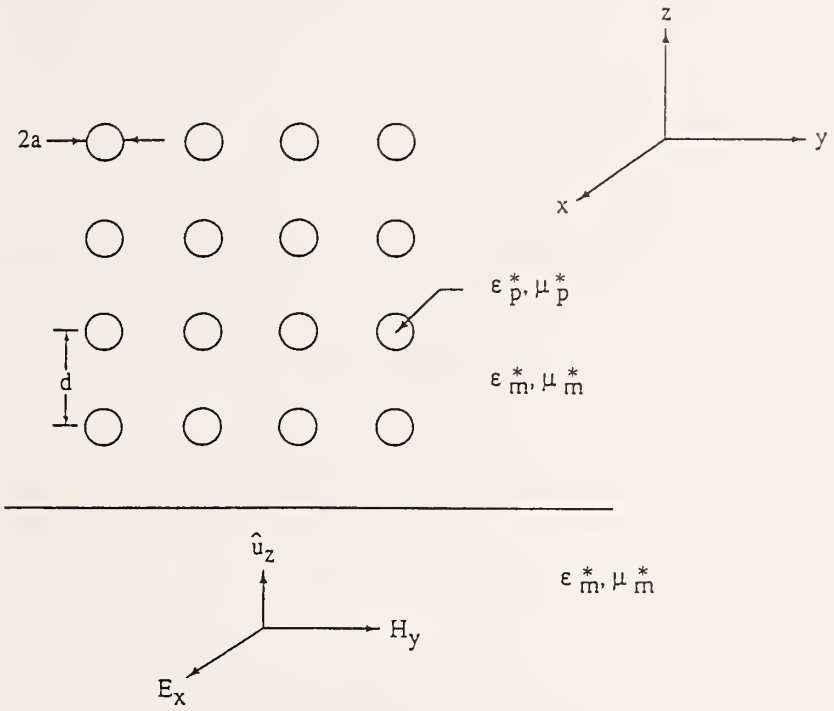

Figure 2.3: Uniform lattice of dispersed dielectric permeable spheres in a dielectric permeable host matrix.

with distance d between centers in a host medium that has arbitrary complex permittivity $\epsilon^*_m = \epsilon'_m(1 - \tan\delta_{e,m})$, and complex permeability $\mu^*_m = \mu'_m(1 - \tan\delta_{m,m})$. (See Fig. 2.3.) In the derivation, general excitation of electric and magnetic dipole sources in the composite are considered and represented in terms of Hertz vectors. The scattered reradiated fields from all the spherical particles are taken into account, which allows for the examination of structural resonant effects (higher-order multipole interactions) between the dispersed inclusions. When the radii of the spherical loading particles become small relative to the host matrix propagation constant ($\mid k_m a \mid \ll 1$, where $k_m = \omega\sqrt{\mu^*_m \epsilon^*_m}$ and $\omega = 2\pi f$ is angular frequency), the dominant contributions to the electric and magnetic fields are those from the induced electric and magnetic dipoles, respectively. This simplifies the formulation of the field components in the composite. In the analysis, an electromagnetic plane wave of unit amplitude and $e^{j\omega t}$ time dependence and with electric field polarized in the x-direction and propagating in the z-direction is considered to be incident upon the matrix loaded with spherical particles. Boundary conditions that must be satisfied are the continuity of the normal electric displacement field and normal magnetic induction field, as well as the tangential electric and magnetic field components at the surface of a spherical loading particle. Application of these boundary conditions to the electric- and magnetic-field components, as expressed in spherical coordinates, yields two coupled integral equations for the total x-directed electric and

y-directed magnetic fields at any point (x, y, z):

$$E_x^t(z) = e^{-jk_m z} + \nu E_x^t(z)\frac{\epsilon_{a,p}^* - \epsilon_m^*}{\epsilon_{a,p}^* + 2\epsilon_m^*} - \frac{3}{2}\nu \int_0^\infty (jk_m \frac{\epsilon_{a,p}^* - \epsilon_m^*}{\epsilon_{a,p}^* + 2\epsilon_m^*} E_x^t(w) + (\frac{\mu_m^*}{\epsilon_m^*})^{\frac{1}{2}} H_y^t(w)\frac{\mu_{a,p}^* - \mu_m^*}{\mu_{a,p}^* + 2\mu_m^*}\frac{\partial}{\partial w})e^{-jk_m|w-z|}dw \quad (2.9)$$

and

$$H_y^t(z) = (\frac{\epsilon_m^*}{\mu_m^*})^{\frac{1}{2}} e^{-jk_m z} + \nu H_y^t(z)\frac{\mu_{a,p}^* - \mu_m^*}{\mu_{a,p}^* + 2\mu_m^*} - \frac{3}{2}\nu \int_0^\infty (jk_m \frac{\mu_{a,p}^* - \mu_m^*}{\mu_{a,p}^* + 2\mu_m^*} H_y^t(w) + (\frac{\epsilon_m^*}{\mu_m^*})^{\frac{1}{2}} E_x^t(w)\frac{\epsilon_{a,p}^* - \epsilon_m^*}{\epsilon_{a,p}^* + 2\epsilon_m^*}\frac{\partial}{\partial w})e^{jk_m|w-z|}dw. \quad (2.10)$$

In eqs (2.9) and (2.10), $\nu = 4\pi a^3/(3d^3)$ is the volumetric loading of the dispersed particles, and $\epsilon_{a,p}^*$ and $\mu_{a,p}^*$ are the *apparent* complex permittivity and complex permeability of the dispersed particles which are related to the true complex permittivity and true complex permeability by a complex penetration factor $G(k_p a)$; i.e., $\epsilon_{a,p}^* = G(k_p a)\epsilon_p^*$ and $\mu_p^* = G(k_p a)\mu_p^*$, where

$$G(k_p a) = 2\frac{\sin(k_p a) - k_p a \cos(k_p a)}{k_p a \cos(k_p a) + (k_p^2 a^2 - 1)\sin(k_p a)} \quad (2.11)$$

and $k_p = \omega\sqrt{\mu_p^* \epsilon_p^*}$. Note that the function modifying the true particle inclusion complex permittivity and permeability is oscillatory and modulates the effective complex electrical and magnetic properties of the composite in a nonobvious manner. The penetration function $G(k_p a)$ is shown as a function of the modulus $\mid k_p a \mid$ in Fig. 2.4. We see that, for various values of $\mid k_p a \mid$, peculiar structural resonant effects are evident in which the effective electrical properties of the composite are not bounded by the individual constituent properties of that composite. The three terms on the right side of eqs (2.9) and (2.10) may be identified as the incident field at z, the scattered field from a spherical particle at the point z, and the scattered field from all the other particles. If the coupled integral equations (2.9) and (2.10) are solved for the effective propagation constant and effective impedance, we obtain the following expression for effective complex permittivity,

$$\epsilon_{eff}^* = \epsilon_m^* \left[1 + \frac{3\nu(\epsilon_{a,p}^* - \epsilon_m^*)}{\epsilon_{a,p}^*(1-\nu) + \epsilon_m^*(2+\nu)}\right]. \quad (2.12)$$

Formally, eq (2.12) is at least consistent and correct in the dilute and dense dispersed suspension extremes. For no loading, $\nu = 0$ and $\epsilon_{eff}^* = \epsilon_m^*$. When there is vanishing

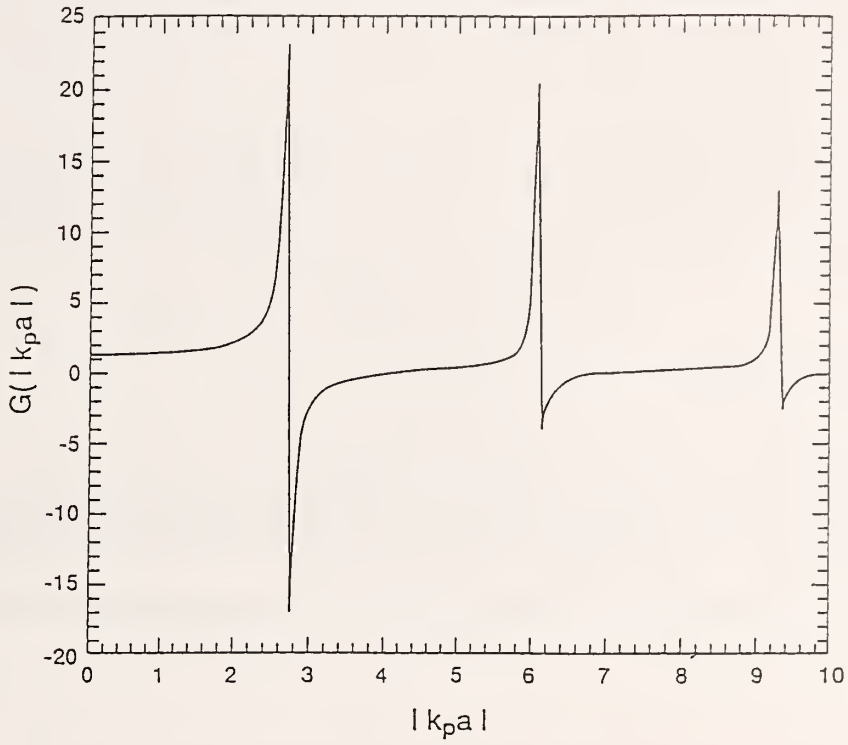

Figure 2.4: Penetration function illustrating effects of particle inclusion size relative to particle inclusion wavenumber on effective electrical properties of composite.

host-matrix material, $\nu \approx 1$ and $\mid k_p a \mid \gg 1$, so that $\epsilon^*_{eff} = \epsilon^*_p$. Although this model intrinsically accounts for higher-order multipole interactions between the dispersed inclusion particles, it is restricted to inclusion sizes that are small relative to a wavelength in the host matrix and to ordered suspension topologies that are uniform and nonpercolating. Its application to composites, where local aggregates or conductive clusters can form together with dispersed suspensions, is questionable.

Chapter 3

Effective-Medium Formulations with Local Particle Aggregates

3.1 Clausius-Mossotti Adaptation to Aggregate Model

The Clausius-Mossotti equation for a suspension of spheres having two differing constitutive electric properties is given in eq (2.3). This equation is valid for topologies involving ordered *island-* or *cermet*-type suspensions. For the Clausius-Mossotti model, the total volume ν of all particles present is given by

$$\nu = \nu_1 + \nu_2, \tag{3.1}$$

and is *less* than the sample volume except when all particles are in aggregates or clusters and the aggregates fill all space. In the latter case, the suspension as a whole would be randomly close-packed. To adapt the "island" topology of the Clausius-Mossotti model to one that includes the formation of aggregates, we define x as being equal to the *total* conductive particle volume fraction and x_1 and x_2 representing the conductive particle volume fractions in isolated spheres and aggregates, respectively. We then have

$$x = x_1 + x_2. \tag{3.2}$$

If the fraction of the conductor content in the aggregates is denoted by f, then

$$x_1 = (1 - f)x, \qquad x_2 = fx. \tag{3.3}$$

We now note that within each isolated spherical inclusion, the volume fraction is unity, whereas the compact aggregates are have a conductor volume fraction equal to the close-packing limit x_c. Hence the volume fractions of the isolated spheres and the aggregates may be written as

$$\nu_1 = (1 - f)x, \qquad \nu_2 = fx(1/x_c). \tag{3.4}$$

The Clausius-Mossotti adaptation to a model that includes both dispersed sphere and aggregate topologies is then [12]

$$\begin{aligned}\frac{\epsilon'_{eff}-1}{\epsilon'_{eff}+2} &= \nu_1\frac{\epsilon'_1-1}{\epsilon'_1+2}+\nu_2\frac{\epsilon'_2-1}{\epsilon'_2+2} \\ &= (1-f)x\frac{\epsilon'_1-1}{\epsilon'_1+2}+fx\left(\frac{1}{x_c}\right)\frac{\epsilon'_2-1}{\epsilon'_2+2}. \end{aligned} \tag{3.5}$$

In order to use eq (3.5) we must either know or make a reasonable statistical assumption about the aggregate fraction f in relation to the total conductor volume fraction x and the close-packing limit x_c. For $x = 0$, $f = 0$ and for $x = x_c$, $f = 1$. If we assume a *linear* relation between these two limits, e.g., $f = x/x_c$, we have

$$\frac{\epsilon'_{eff}-1}{\epsilon'_{eff}+2} = \left(1-\frac{x}{x_c}\right)x\frac{\epsilon'_1-1}{\epsilon'_1+2}+\left(\frac{x}{x_c}\right)^2\frac{\epsilon'_2-1}{\epsilon'_2+2}. \tag{3.6}$$

Solving for ϵ'_{eff},

$$\epsilon'_{eff} = \frac{N_{C-M}}{D_{C-M}}, \tag{3.7}$$

where

$$\begin{aligned} N_{C-M} &= x_c^2(\epsilon'_1+2)(\epsilon'_2+2)-2x^2\left[\epsilon'_1(\epsilon'_2(x_c-1)+2x_c+1)-\epsilon'_2(x_c+2)-2(x_c-1)\right] \\ &\quad -2x_c^2x(1-\epsilon'_1)(\epsilon'_2+2) \end{aligned} \tag{3.8}$$

and

$$\begin{aligned} D_{C-M} &= x_c^2(\epsilon'_1+2)(\epsilon'_2+2)+x^2\left[\epsilon'_1(\epsilon'_2(x_c-1)+2x_c+1)-\epsilon'_2(x_c+2)-2(x_c-1)\right] \\ &\quad +x_c^2x(1-\epsilon'_1)(\epsilon'_2+2). \end{aligned} \tag{3.9}$$

If we treat both ϵ'_1 and ϵ'_2 as large relative to unity in eq (3.5), we may write

$$\frac{\epsilon'_{eff}-1}{\epsilon'_{eff}+2} = (1-f)x+fx(\frac{1}{x_c}). \tag{3.10}$$

Again, for well-stirred samples, $f = 0$ at $x = 0$ and $f = 1$ at $x = x_c$, so that, with $f = x/x_c$,

$$\begin{aligned}\frac{\epsilon'_{eff}-1}{\epsilon'_{eff}+2} &= \frac{x\left[x_c^2+x\left(x_c-1\right)\right]}{x_c^2} \\ &= x\left[1+\frac{x}{x_c}\left(\frac{1}{x_c}-1\right)\right]. \end{aligned} \tag{3.11}$$

Hence

$$\epsilon'_{eff} = \frac{3x_c^2}{x^2(x_c-1)-x_c^2(x-1)}-2. \tag{3.12}$$

3.2 Bruggeman Adaptation to Aggregate Model

The Bruggeman relation for a two-phase medium composed of spherical elements is

$$V_1 \frac{\epsilon_1' - \epsilon_{eff}'}{\epsilon_1' + 2\epsilon_{eff}'} + V_2 \frac{\epsilon_2' - \epsilon_{eff}'}{\epsilon_2' + 2\epsilon_{eff}'} = 0. \tag{3.13}$$

The volume fractions V_1 and V_2 differ from ν_1 and ν_2 since they apply to suspensions of different topologies. Because an implicit assumption of the Bruggeman model is that the phases are very close together with negligible interstices, the sum of the volumes *must* fill the sample volume so that

$$V_1 = 1 - V_2. \tag{3.14}$$

The Bruggeman model is clearly not applicable to a monodisperse suspension of spherical elements, since such a suspension cannot fill sample volume space, even at closest packing density. An artifact of the Bruggeman model is to use a heterodisperse set of suspensions of ever smaller spheres so that, in the limit, all sample volume space is filled. This is not a useful artifact to employ when we are dealing with an actual monodisperse suspension of spheres. Our suspension consists of monodisperse isolated conductive spheres and compact conductive aggregates of spheres. The aggregates are not necessarily spherical in themselves, but may form irregular conductive regions that are intermingled with similarly irregular dielectric regions containing the remaining unclustered spheres (see Fig. 2.2). However, both the dielectric insulating and conductive regions individually do satisfy the assumptions of the Bruggeman's model. Hence we can treat regions 1 and 2 of the (effective) suspension as an intermingled mixture of dielectric (region 1) and conductor (region 2) phases. The aggregate fraction will still be f and the critical volume fraction for closest random packing will still be x_c. Instead of being the volume fractions of particle types 1 and 2, as in the Clausius-Mossotti model, the V_1 and V_2 in the adapted Bruggeman model will be taken as *region* volume fractions. In this case, we still have

$$x_1 = (1 - f)x, \qquad x_2 = fx, \tag{3.15}$$

and

$$x_2 = fx = x_c V_2, \tag{3.16}$$

as long as f is the aggregate or clustered volume fraction and x_c represents the close-packed volume fraction of the conductive phase in terms of actual conductor volume fraction. From eq (3.4),

$$V_2 \;=\; fx\left(\frac{1}{x_c}\right). \tag{3.17}$$

Because the conductor phase is close-packed, $\nu_2 \equiv V_2$. However, the dielectric phase is *not* close-packed, so that $\nu_1 \neq V_1$; rather, from eq (3.14),

$$V_1 = 1 - fx\left(\frac{1}{x_c}\right). \tag{3.18}$$

Because we are using the Bruggeman model to model the *regions* of conductive dispersed and clustered phases, we require the actual conductor volume fraction in region 1 relative to the volume of region 1. From eq (3.18) this is

$$x'_{region1} = \frac{x_1}{V_1} = \frac{(1-f)x}{1 - fx(1/x_c)}. \tag{3.19}$$

Equation (3.19) may then be used in the (island) Clausius-Mossotti relation to determine the effective permittivity of the unclustered dielectric region 1, after which the Bruggeman relation is applied to both regions 1 and 2 to determine the effective permittivity of the composite. The effective permittivity of region 1 is then given by

$$\epsilon'_{eff,region1} = 1 + \frac{3x'_{region1}}{1 - x'_{region1}}. \tag{3.20}$$

If eq (3.20) is used in eq (3.13), a rather complex quintic polynomial results when attempting to solve for the effective permittivity in terms of ϵ'_2. However, this equation simplifies considerably when the permittivity ϵ'_2 is large relative to unity. The Bruggeman relation simplifies to

$$\frac{(1 - f\frac{x}{x_c})(\epsilon'_{eff,region1} - \epsilon'_{eff})}{\epsilon'_{eff,region1} + 2\epsilon'_{eff}} + f\frac{x}{x_c} = 0, \tag{3.21}$$

yielding

$$\epsilon'_{eff} = \frac{\epsilon'_{eff,region1}}{1 - 3x/x_c}. \tag{3.22}$$

3.3 Maxwell-Garnett Adaptation to Aggregate Model

The Maxwell-Garnett mixing rule, given in eq (2.4), is also known as the *Rayleigh mixing formula* [13]. The Rayleigh rule does not contain information about an individual scatterer; rather, only the volume fraction ν_1 of the inclusion phase and the permittivities of the inclusion phase ϵ'_1 and host ϵ'_m appear in the mixing rule.

The Maxwell-Garnett mixing formula yields eq (2.5) for the effective permittivity of the composite, which may be written in the following form:

$$\epsilon'_{eff} = \epsilon'_m + 3\nu_1\epsilon'_m \frac{\epsilon'_1 - \epsilon'_m}{\epsilon'_1 + 2\epsilon'_m - \nu_1(\epsilon'_1 - \epsilon'_m)}, \tag{3.23}$$

or

$$\frac{\epsilon'_{eff}}{\epsilon'_m} = 1 + 3\nu_1 \frac{\frac{\epsilon'_1}{\epsilon'_m} - 1}{\frac{\epsilon'_1}{\epsilon'_m} + 2 - \nu_1(\frac{\epsilon'_1}{\epsilon'_m} - 1)}. \tag{3.24}$$

We note that, when $\nu_1 \to 0$, the effective permittivity reduces to that of the matrix, and when $\nu_1 \to 1$, the effective permittivity reduces to that of the inclusion phase. The only way that the condition $\nu_1 \approx 1$ can be achieved, however, is that a polydisperse suspension of spherical inclusions be permitted. Sihvola [3] gives useful insight into the average electric fields internal and external to spherical inclusions and their relation to the Maxwell-Garnett rule by defining the effective macroscopic permittivity of a 2-phase composite as a constant relating the volume-averaged electric field $< \mathbf{E} >$ and displacement field flux density $< \mathbf{D} >$; that is,

$$< \mathbf{D} >= \epsilon^*_{eff} < \mathbf{E} >, \tag{3.25}$$

where $\epsilon^*_{eff} = \epsilon'_{eff}(1 - j \tan \delta_{eff})$, ϵ'_{eff} is the effective real permittivity, and $\tan \delta_{eff}$ is the effective dielectric loss tangent. The average electric field and displacement flux density are then written in terms of the corresponding volume fractions and the electric fields internal, $\mathbf{E}_i$, and external, $\mathbf{E}_e$, to the inclusions:

$$< \mathbf{E} >= f\mathbf{E}_i + (1 - f)\mathbf{E}_e \tag{3.26}$$

and

$$< \mathbf{D} >= f\epsilon_i\mathbf{E}_i + (1 - f)\epsilon_e\mathbf{E}_e, \tag{3.27}$$

where ϵ_i and ϵ_e are the complex permittivities of the inclusions and the matrix host. From eqs (3.26) and (3.27),

$$\begin{aligned} \frac{< \mathbf{D} >}{< \mathbf{E} >} &= \epsilon_{eff} \\ &= \frac{f\epsilon_i \frac{\mathbf{E}_i}{\mathbf{E}_e} + (1 - f)\epsilon_e}{f\frac{\mathbf{E}_i}{\mathbf{E}_e} + (1 - f)}. \end{aligned} \tag{3.28}$$

For spherical, isotropic inclusions, only an equivalent dipole source exists for each inclusion, and the polarizability is a scalar that does not depend on the direction of the electric field, but only on its amplitude. If we assume for this case that the ratio between the internal electric field and external electric field is approximately the same as the quasi-static case, Sihvola [3] has shown that

$$\frac{|\mathbf{E}_i|}{|\mathbf{E}_e|} = \frac{3\epsilon_e}{\epsilon_i + 2\epsilon_e}. \tag{3.29}$$

Direct substitution of eq (3.29) into eq (3.28) yields

$$\epsilon_{eff} = \epsilon_e + 3f\epsilon_e \frac{\epsilon_i - \epsilon_e}{\epsilon_i + 2\epsilon_e - f(\epsilon_i - \epsilon_e)}, \tag{3.30}$$

which is identical to the Maxwell-Garnett mixing formula, eq (3.23).

We may now adapt the Maxwell-Garnett mixing rule using the same technique as performed with the Bruggeman and Clausius-Mossotti topologies. This is done by assuming that the effective permittivity of the carbon-clustered region may be adequately given by a carbon host phase with silicone inclusions, where the volume fraction of the carbon in the clusters is the Bernal maximum random-packing limit for equal-sized spherical inclusions. In the unclustered region, the Maxwell-Garnett rule is used with the opposite topology. Then a composite permittivity is given by

$$\epsilon_{eff} = \frac{V_1 c_1 \epsilon_1 + V_2 c_2 \epsilon_2 + V_3 c_3 \epsilon_3}{V_1 c_1 + V_2 c_2 + V_3 c_3}, \tag{3.31}$$

where $V_1 = 1 - x(1 - x/x_c) - (x/x_c)^2$, $V_2 = x(1 - x/x_c)$, $V_3 = (x/x_c)^2$, $c_1 = 1/3$, $c_2 = \epsilon_1/(2\epsilon_1 + \epsilon_2)$, $c_3 = \epsilon_1/(2\epsilon_1 + \epsilon_3)$, x is the total volume fraction of carbon, and $x_c = 0.63$ is the maximum volume filling factor. With the Maxwell-Garnett rule, the permittivity of the carbon cluster region with a carbon host and silicone inclusions is given by

$$\epsilon_3 = \frac{\epsilon_1[\epsilon_1(3 - 2x_c) + 2x_c\epsilon_2]}{[x_c\epsilon_1 + \epsilon_2(3 - x_c)]}. \tag{3.32}$$

In Fig. 3.1 the respective volume fractions V_1, V_2, and V_3 for the host silicone, the unclustered carbon, and the clustered carbon are illustrated as a function of total volume fraction of the carbon in the composite. These volume fractions are plotted using the packing fraction limit of 0.63 for randomly organized spheres.

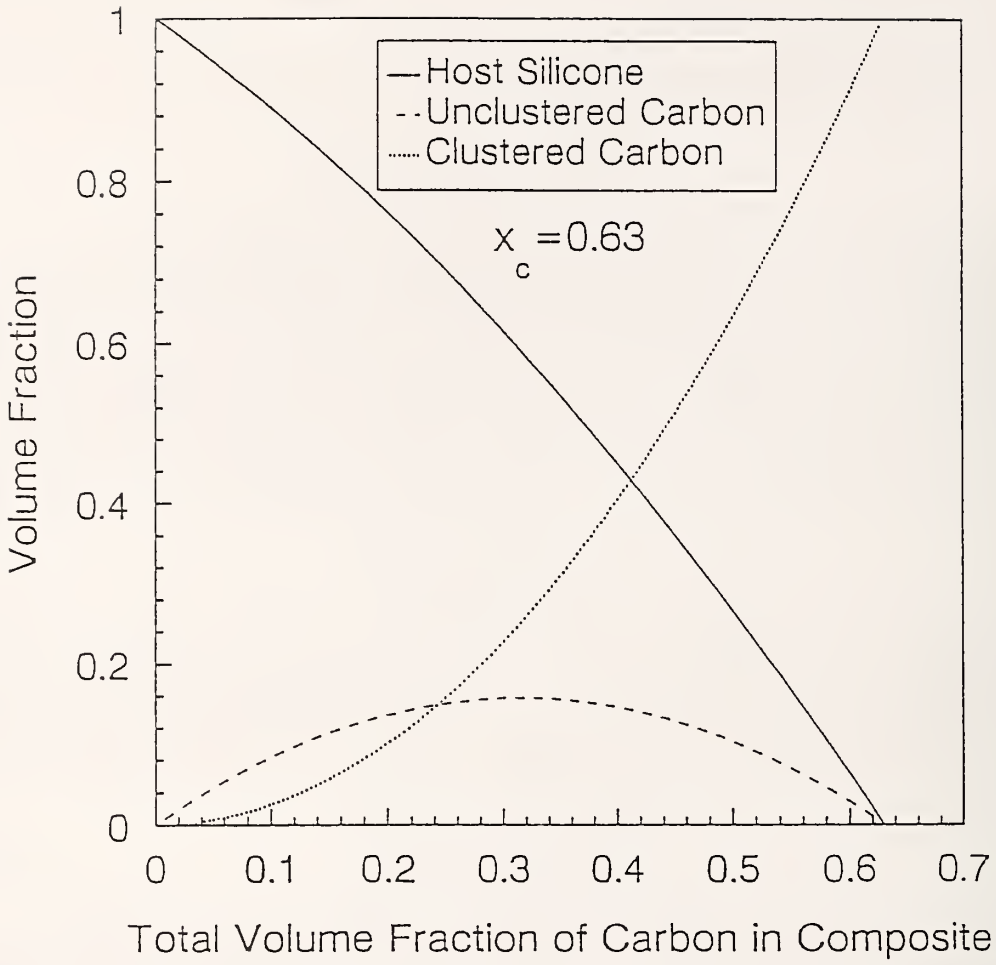

Figure 3.1: Volume fractions of host silicone, unclustered carbon, and clustered carbon in composite as function of total volume fraction of carbon in composite.

Chapter 4

Measurements and Theory

The conductivities and permittivities of carbon-black-loaded polymer composites were measured at frequencies from 1000 Hz to 1 MHz with an open-circuit coaxial holder. This fixture consists of an open-circuited 14 mm coaxial line with the center conductor shorter than the outer-conductor shield. The shielded open-circuited holder is quite useful for measuring the dielectric properties of powders, liquids, and semisolids because of the ease of sample insertion. Previous dielectric measurements performed using the shielded open-circuited sample holder are described in the literature [14-22]. A rigorous treatment of the fringing capacitance at the open-circuited termination has been given in [1]. The reflection coefficient of the transmission line was measured using an automatic network analyzer. Alternatively, the line capacitance and conductance were measured using an LCR meter.

Spherical carbon-black pearls, having individual particle sizes of 12 nm, were mechanically stirred with silicone, and temperature annealing was required to stabilize the carbon-black silicone composite [1]. A study of how percolation at thermodynamic equilibrium is correlated to dynamic percolation under differing experimental temperatures and annealing times in carbon-black-filled polymer composites has been given by Wu, Asai, Zhang, Miura, and Sumita [23]. Real relative permittivity and conductivity data of this composite at 800 kHz for various volume fraction carbon loading are shown in Figs. 4.1 and 4.2. Both the real permittivity and conductivity increase rapidly when the carbon volume fraction exceeds 0.2, which is a volume fraction well below the close-packing limit. The predicted normalized composite permittivity from the well stirred Clausius-Mossotti cluster model and the Bruggeman cluster model as a function of carbon loading are compared in Fig. 4.3. The Maxwell-Garnett adaptation that accounts for aggregation or clustering of conductor particles in a conductor-insulator composite has a percolation threshold similar to that of the Clausius-Mossotti aggregate model. This can be seen in Fig. 4.4, where calculated real permittivities of carbon-black-loaded

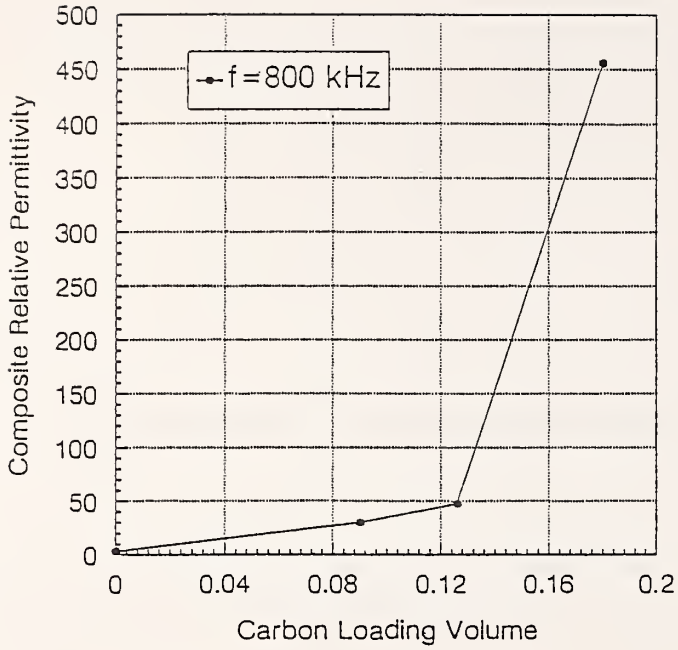

Figure 4.1: Real relative permittivity of carbon-black pearl and silicone composites as a function of carbon loading. Frequency and temperature are 800 kHz and 22 °C. After [1].

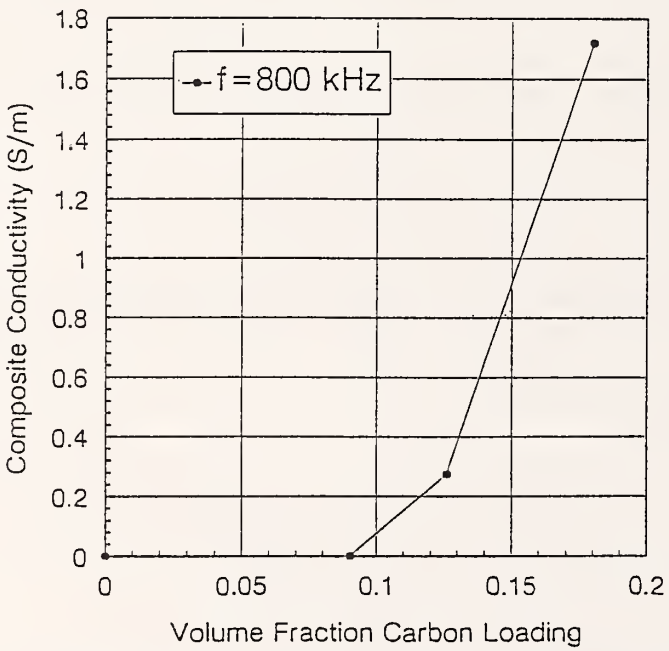

Figure 4.2: Conductivity of carbon-black pearl and silicone composites as a function of carbon loading. Frequency and temperature are 800 kHz and 22 °C. After [1].

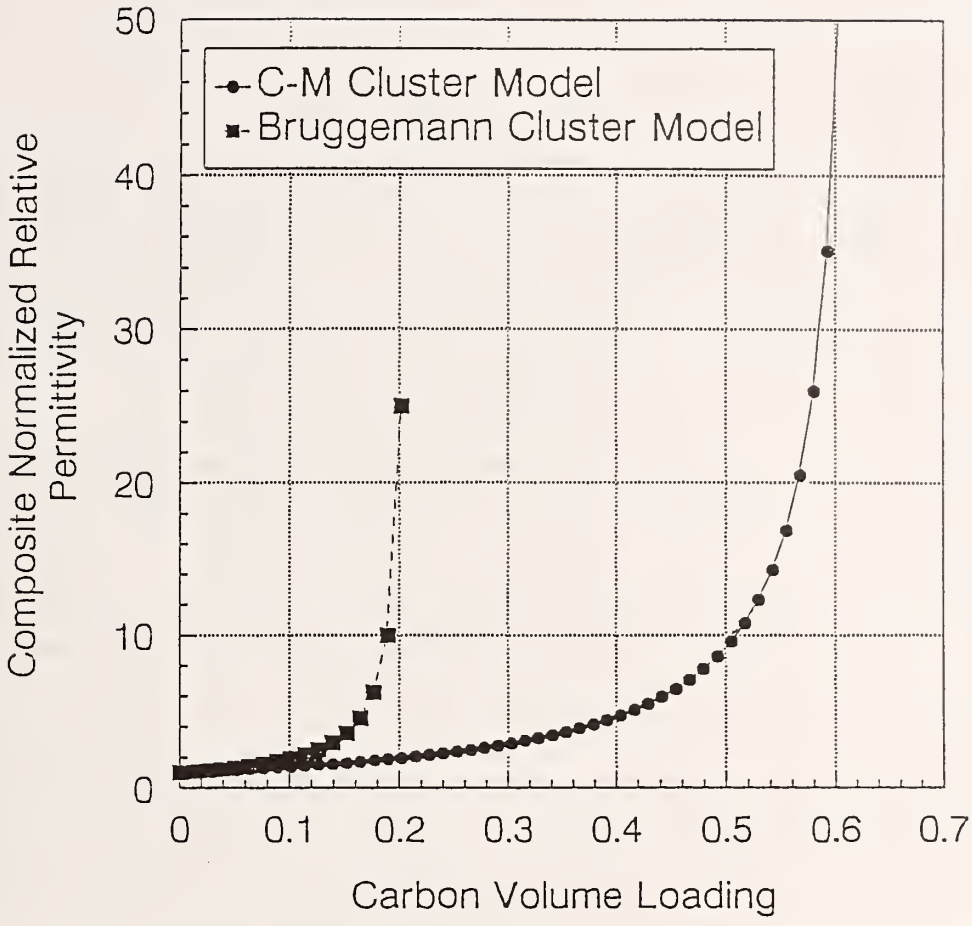

Figure 4.3: Normalized composite real permittivity (or normalized composite conductivity) as a function of conductor-particle volume loading x for differing disordered suspensions. The solid line is the reduced permittivity (or conductivity) given by the Clausius-Mossotti aggregate model, reflecting well stirred composite samples, with cluster fraction $f = x/x_c$. The dashed line is the normalized real permittivity (or normalized conductivity) given by the Bruggeman aggregate cluster model, with cluster fraction $f = 1$. All calculations use Bernal's experimental value for random closest packing of spherical particles, $x_c = 0.63$. Note that the percolation threshold for the Clausius-Mossotti aggregate model occurs where $x = x_c = 0.63$, whereas for the Bruggeman aggregate model, the percolation threshold occurs well below the close-packing limit at $x = x_c/3 = 0.21$.

silicone composites using the Maxwell-Garnett aggregate model (eq (3.30)) are shown as a function of total volumetric carbon loading. The Bruggeman aggregate predictive model, showing the normalized permittivity (or conductivity) as a function of carbon loading for differing parametric cluster fractions, is given in Figs. 4.5 and 4.6. The same percolation threshold is evident for all total volumetric metal particle loadings, but the normalized permittivities or conductivities can vary with carbon loading at values below the percolation threshold, depending on the cluster volume fraction.

Comparison of these predictive model considerations, which incorporate aggregates or localized clusters of the conductor (carbon) loading particles, indicate that the adapted Bruggeman aggregate model appears to best fit our laboratory data on the composite phantom materials, as presently fabricated (where percolation begins well below the close-packing limit). A range of carbon black loading $0 \leq x \leq 0.15$ in the silicone provides a suitable conductivity range for phantom materials that would simulate most body tissues (see Fig. 1.1) so that we can, in principle, simulate all human body tissues with various carbon-black-loaded silicone composites. Better reproducibility of the low-frequency electrical properties of the carbon-black-loaded silicone composites could be obtained by forcing the percolation threshold to occur at higher carbon volumetric loadings near the close-packing limit. This type of carbon suspension topology requires well-stirred sample fabrication.

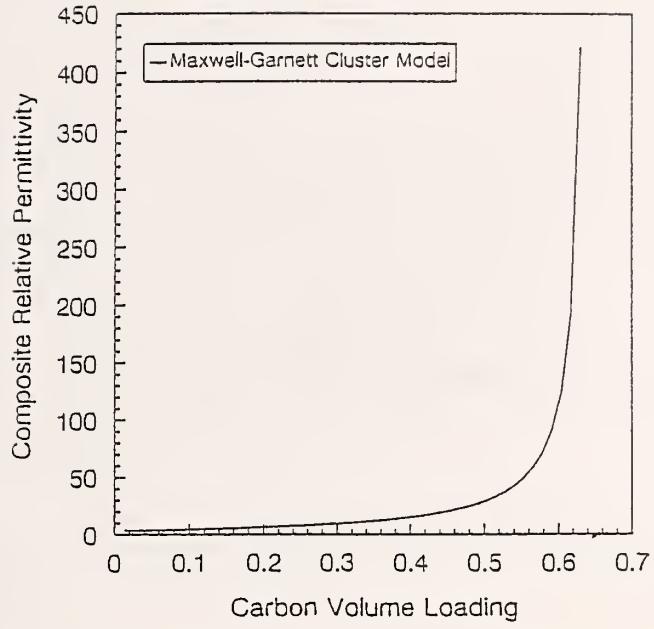

Figure 4.4: Predicted real permittivity of carbon-black-loaded silicone composite with Maxwell-Garnett aggregate model. Real relative permittivities of 3.37 for silicone and 788 for carbon black were used in calculations. Note that with this model the percolation threshold occurs at the close-packing limit, $x = x_c$=0.63.

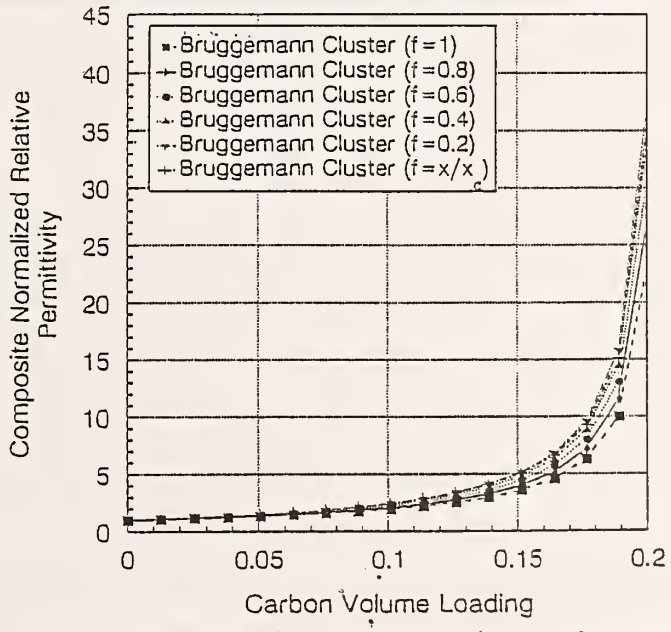

Figure 4.5: Composite normalized permittivity (or conductivity) as a function of conductor-particle loading and cluster fraction with Bruggeman aggregate model.

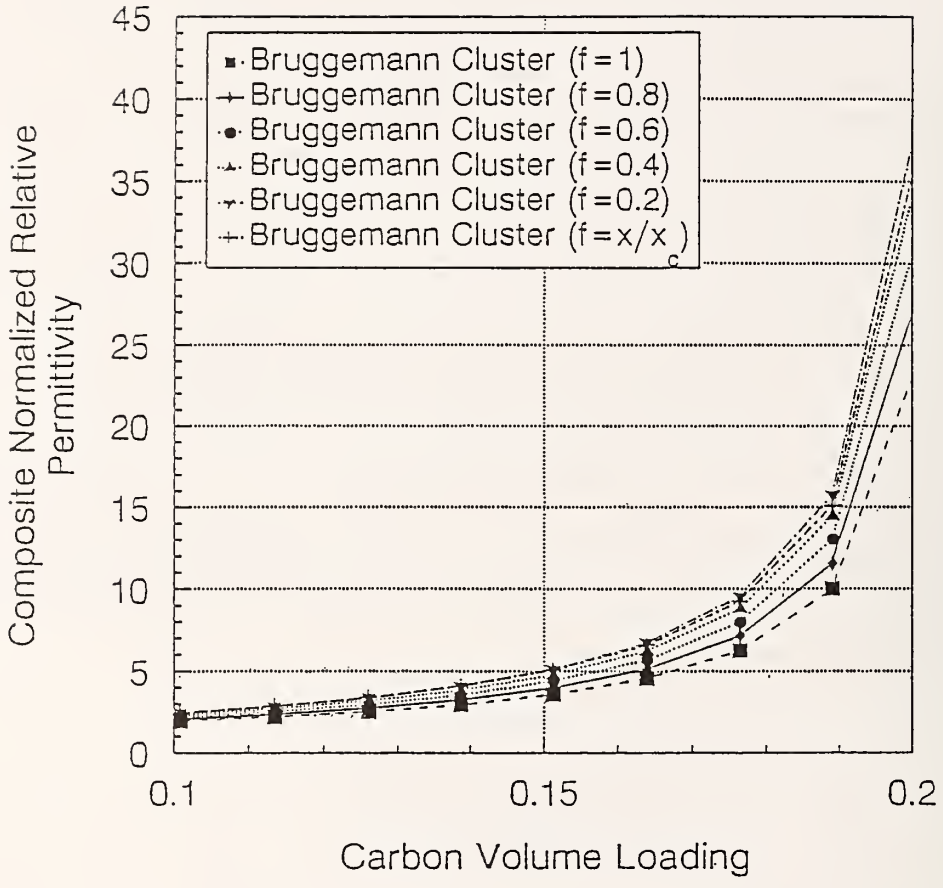

Figure 4.6: Windowed normalized permittivity (or conductivity) as a function of conductive particle loading and cluster fraction using Bruggeman aggregate model.

Chapter 5

Conductivity Temperature Dependence of Carbon-Black-Filled Polymers

Polarization processes occurring in materials can be strong functions of both frequency f and absolute temperature T (K). The dependence of conductivity on frequency for various carbon-black-loaded silicone composites that are useful for simulating biologic phantom materials has been reported previously from 1000 Hz to 1 MHz [1]. The room-temperature experimental conductivity data demonstrate little frequency dependence over the frequency range of most metal detection systems, which is an important criterion when selecting phantom biologic models to be used for assessing the sensitivity of metal detectors.

5.1 General Effect of Temperature Changes

In order to gain insight into temperature-dependent variations of the effective complex dielectric permittivity over the frequency range where dipolar or orientation phenomena occur, we can usefully consider concepts borrowed from statistical thermodynamics [24]. If the polarizability of a material at a given temperature and under the influence of a time-varying electric field can be related to the known (measured) activation energy U of that material, then we can derive a method for predicting the dielectric behavior of that material as a function of temperature. Of course, this predictive ability will be constrained by the assumptions implicit in the physical model and must be validated by measurements of the dielectric permittivity and conductivity as a function of temperature.

Consider a bistable model of an elementary dipole within a dielectric whose molecular

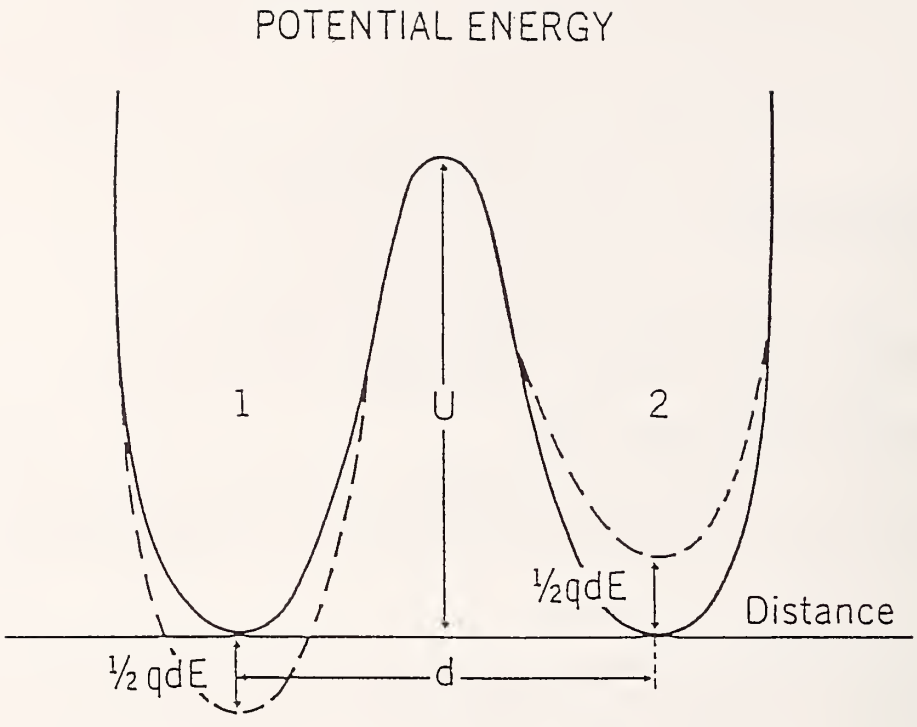

Figure 5.1: Potential energy of a bistable model having two minima, depicted by states 1 and 2. The depths of these minima are modified by an applied electric field, and charged particles can occupy either state [26].

groupings can be characterized by well defined permanent dipole moments. In this type of model, we assume that a charge q may be in one of two states that are separated be a distance d. These states are portrayed in Fig. 5.1. In this model, an electric field acting on the dielectric causes movement of charge from the minimum of state 1 to the minimum of state 2. This charge movement is equivalent to a 180° rotation of a dipole of moment

$$| \vec{p} | = \frac{1}{2} qd. \tag{5.1}$$

The potential difference due to the applied electric field $\vec{E}$ is simply

$$\psi_1 - \psi_2 = 2\vec{p} \cdot \vec{E} = qdE \cos\theta, \tag{5.2}$$

where θ is the angle between the direction of the electric field and the dipole moment.

The interaction between individual dipoles within the dielectric may be neglected by assuming that the total number N of bistable dipoles per unit volume is small. This

would correspond to levels of carbon-black loading in the polymer below the percolation threshold. For dipoles we may also generally assume that $\theta = 0$ and that equal potential energy exists for states 1 and 2 in the absence of an electric field. We can visualize this microscopic assembly in which the bistable dipoles are in a heat reservoir which consists of spontaneously active particles that exchange energy through thermal fluctuations with each other and the dipoles. Therefore, the directions of the dipoles fluctuate. Occasionally, thermal fluctuations allow a charge located in the minimum of state 1 to acquire sufficient energy to go "over" the potential hill U and drop into the minimum of state 2. In state 2, the energy of the charge is returned to the heat reservoir and stays in state 2 until it acquires enough energy from the reservoir to return to state 1.

The probability that a charge may jump in a double potential well (state) has been derived and is well known in classical statistical thermodynamics. Here, we can state that the number of dipoles jumping per unit of time from state 1 to state 2 is given in terms of the difference of potential energy between the two wells as:

$$u_{12} = Ae^{-(U \pm pE)/kT}, \tag{5.3}$$

where k is Boltzmann's constant (1.3807×10^{-23} J/K). The constant A may or may not depend on temperature. Generally, for ionic solids it does not, whereas for organic polymers, A is inversely proportional to T. The $\pm$ signs within the exponential of eq (5.3) dictate whether the minimum in state 2 is lower or higher than that of state 1. Generally, $U \gg kT$.

For dipoles in normal dielectrics, p is of the order 10^{-29} C·m, whereas E for fields below breakdown strength is always less than 10^6 V/m. Therefore, in general,

$$\frac{pE}{kT} \ll 1. \tag{5.4}$$

Note that $pE/(kT)$ is dimensionless and that, as $T \to \infty$, thermal fluctuations dominate polarization, whereas when $T \to 0$, polarization (pE) dominates. Equation (5.3) may approximately be written as

$$u_{12} \approx u(1 - \frac{pE}{kT}), \tag{5.5}$$

where

$$u = Ae^{-U/kT} \tag{5.6}$$

is the frequency of jumps in the absence of an applied electric field. Similarly, the frequency of jumps from state 2 to state 1 can be written in linear form as

$$u_{21} \approx u(1 + \frac{pE}{kT}). \tag{5.7}$$

Provided that the number of charges N_1 jumping from state 1 to state 2 per unit of time is the same as that jumping from state 2 to state 1, N_2, the average population

of charges in the wells of states 1 and 2 will not change with time. In other words, at equilibrium

$$N_1 u_{12} = N_2 u_{21}. \tag{5.8}$$

The total number of bistable dipoles is constant or

$$N_1 + N_2 = N. \tag{5.9}$$

Equations (5.8) and (5.9) allow us to calculate N_1 and N_2 in equilibrium. Since the polarization per unit volume P is defined as that number of dipoles acting in one direction which is not compensated by dipoles acting in the opposite direction, or

$$P = P_s = (N_1 - N_2)p, \tag{5.10}$$

we have a basis from statistical thermodynamics for determining the variation of polarization with temperature when the dielectric is in equilibrium; that is, from eq (5.8),

$$N_1 u(1 - \frac{pE}{kT}) \quad = \quad N_2 u(1 + \frac{pE}{kT})$$

or

$$N_1 - N_2 = (N_1 + N_2)\frac{pE}{kT} = N\frac{pE}{kT}. \tag{5.11}$$

Hence eq (5.10) may be written as

$$P_s = N\frac{p^2 E}{kT}. \tag{5.12}$$

We are now in a position to derive the frequency-dependent properties of the model. We note that the change in number of dipoles in state 1 is equal to the outflow number to state 2 less the inflow number from state 2; or

$$\frac{dN_1}{dt} = -N_1 u_{12} + N_2 u_{21}. \tag{5.13}$$

Since the total number of bistable dipoles is constant,

$$\frac{dN_1}{dt} \quad = \quad -\frac{dN_2}{dt};$$

or

$$\frac{d(N_1 - N_2)}{dt} = 2\frac{dN_1}{dt}, \tag{5.14}$$

so that eq (5.13) becomes

$$\begin{aligned} \frac{dN_1}{dt} &= \frac{1}{2}\frac{d(N_1 - N_2)}{dt} \\ &= -N_1 u(1 - \frac{pE}{kT}) + N_2 u(1 + \frac{pE}{kT}). \end{aligned} \tag{5.15}$$

Equation (5.15) can be simplified to read

$$\frac{1}{2}\frac{d[N_1 - N_2]}{dt} = -u(N_1 - N_2) + u(N_1 + N_2)\frac{pE}{kT} \tag{5.16}$$

or

$$\frac{1}{2}\frac{d[(N_1 - N_2)p]}{dt} = -u(N_1 - N_2)p + uN\frac{p^2E}{kT}. \tag{5.17}$$

We now have a differential equation for the dipolar polarization of a dielectric medium as a function of temperature; that is

$$\frac{1}{2u}\frac{dP}{dt} + P = \frac{Np^2E}{kT}. \tag{5.18}$$

This equation is very similar to that for a dielectric medium that has a single relaxation time [24]; in other words, eq (5.18) is a relaxation equation with a relaxation time

$$\tau = \frac{1}{2u} = \frac{1}{2A}e^{U/kT}, \tag{5.19}$$

so that we may generalize eq (5.18) to

$$\tau\frac{dP_D}{dt} + P_D = \alpha_D E, \tag{5.20}$$

where P_D is the dipolar polarization and α_D is the dipolar polarizability of the dielectric material. Using simple Fourier-transform methods we obtain the following expressions for the complex permittivity $\epsilon^*(\omega,T) = \epsilon'(\omega,T) - j\epsilon''(\omega,T) = \epsilon_0\epsilon_r'(1 - \tan\delta)$:

$$\epsilon^*(\omega,T) - \epsilon_\infty(T) = \frac{\alpha_D}{1 + j\omega\tau}, \tag{5.21}$$

or

$$\epsilon'(\omega,T) = \epsilon_\infty(T) + \frac{\alpha_D}{1 + \omega^2\tau^2}, \tag{5.22}$$

$$\epsilon''(\omega,T) = \frac{\alpha_D\omega\tau}{1 + \omega^2\tau^2}, \tag{5.23}$$

and

$$\tan\delta(\omega,T) = \frac{\alpha_D\omega\tau}{\alpha_D + \epsilon_\infty(T)(1 + \omega^2\tau^2)}, \tag{5.24}$$

where $\omega = 2\pi f$, ϵ_∞ is the optical dielectric constant defined by the simple relation $\epsilon_\infty - 1 = n^2 - 1 = P_\infty/E$, n is the refractive index of the material, and P_∞ is the optical polarization. The dependence of conductivity on frequency is given by

$$\sigma = \omega\epsilon_0\epsilon_r''. \tag{5.25}$$

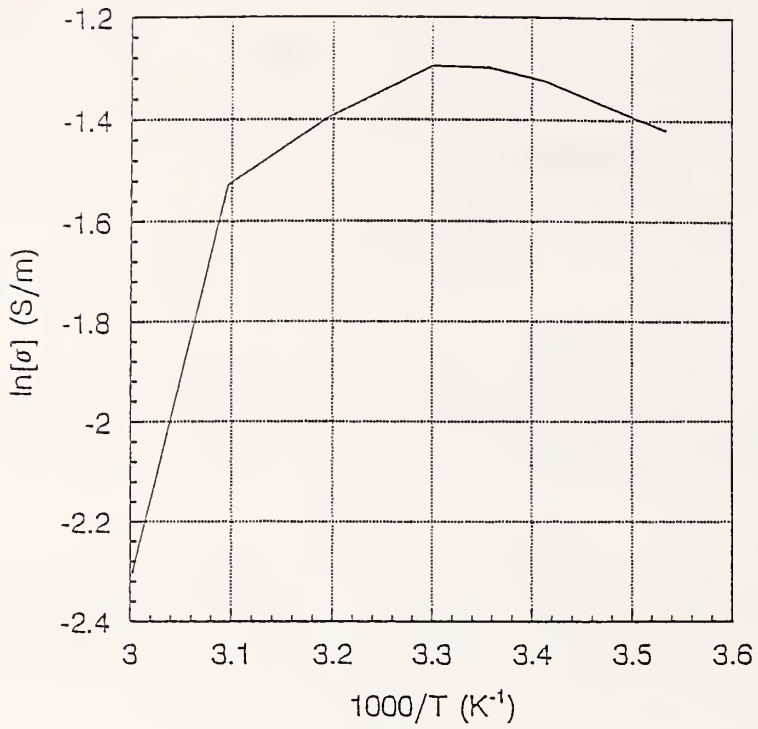

Figure 5.2: Log conductivity versus 1000/T for a carbon black-loaded silicone composite with loading of 7 % by weight. Data shown are average log-conductivity values for the frequency range 1 kHz to 1 MHz.

Equations (5.21-5.25) describe dispersive dielectric behavior for a bistable dielectric as a function of temperature and frequency. The temperature-dependent permittivity and conductivity are given in terms of the dipolar polarizability, activation energy, and high-frequency (optical) permittivity at temperature T. The derivation is limited to dielectric materials where interaction between individual dipoles can be neglected, and for conditions where $pE \ll kT$ (nonsuperconducting states).

5.2 Variable-Temperature Measurements on Carbon- Black Conductive Polymers

Variable-temperature measurements of conductivity were performed with the shielded open-circuited sample holder. The shielded open-circuited measurement system was placed in an environmental chamber which operates from −150 °C to 350 °C. This chamber has feed-through bulkhead adapters on the sides for passage of coaxial rf feeds to the measurement system being used [25]. In addition, the chamber has purging ports for injecting nitrogen gas, either to reduce water vapor or to reduce oxidation in the chamber. The derived conductivity data obtained from these reflection measurements are shown as an Arrhenius plot in Fig. 5.2.

In general, the conductivity σ (S/m) for an Arrhenius process is

$$\sigma = \sigma_0 e^{-U/kT}, \tag{5.26}$$

where σ_0 is a reference conductivity. Equation (5.26) can be written as $\ln\sigma - \ln\sigma_0 = -U/(kT)$. We may suppress the reference value $\ln\sigma_0$ and simply plot $\ln\sigma$ versus $1/T$ to determine the activation energy U, since $\ln\sigma_0$ acts only to shift functional values of $\ln\sigma$ on the ordinate. An Arrhenius plot allows us to predict the conductivity temperature dependence expected for the carbon black conductive polymer composite under the influence of a time-varying electric field.

Plots of measured temperature-dependent conductivity can also allow us to evaluate conductivity mechanisms associated with differing high- and low-temperature processes in the composite. For example, two Arrhenius processes with different temperature-dependent activation energies may be summed as

$$\sigma = \sigma_1 e^{-U_1/(kT)} + \sigma_2 e^{-U_2/(kT)}; \tag{5.27}$$

the respective slopes of $\ln(\sigma/\sigma_1)$ or $\ln(\sigma/\sigma_2)$ versus $1/T$ would yield the sum of the two activation energies for the two processes associated with two differing conduction mechanisms. Activation energies for high-temperature conduction processes are greater than those for low-temperature processes. Knowledge of the conduction mechanisms can, within practical limits, permit the engineering of conductivity of the composite, or at least constrain the temperature variability of conductivity in the composite.

The data shown in Fig. 5.2 were taken over a limited temperature range; i.e., from 10 °C to 60 °C (283 to 333 K), which, in general, exhibit conductivity variations associated with high-temperature processes. The temperature behavior of the conductivity for the carbon-black composite from 10 to 25 °C (283 to 298 K) is similar to that of an extrinsic, partially compensated n-type semiconductor [27]. For an extrinsic n-type semiconductor, the high-temperature process is associated with conductivity in the conduction band. If measurements were taken at much lower temperatures, we would expect a second Arrhenius conduction process having lower activation energy associated with nearest-neighbor hopping of electrons from occupied to unoccupied sites. However, a very strong *reversal* of this conductivity increase with increasing temperature is apparent at temperatures greater than 40 °C (313 K). The carbon-black conductive polymer composite has changed from one that has a negative temperature coefficient of resistance to one that has a very large positive temperature coefficient (PTC) of resistance, or one which exhibits a very large increase of resistance at temperatures above 40 °C. The large PTC of carbon-black-filled polymers above room temperature has been observed by Carmona and Ravier [28].

This phenomenon can be explained physically in the following way. The 7 % by weight carbon-black-loaded polymer is close to the expected percolation threshold, as

predicted by the aggregate adaptation of the Bruggeman rule. As temperature is increased above 40 $^{\circ}C$, the thermal expansion of the composite itself induces changes in the correlation lengths of the clustered carbon. In other words, the carbon particles are likely disconnected, causing the composite to exhibit non-percolative behavior and a very large PTC.

Materials having high PTC can be used in important applications such as self-regulated heaters and electrical safety devices. For biologic phantom model applications, temperatures should be kept below 40 °C in order to maintain required conductivity values that simulate body tissues.

Chapter 6

Summary

Carbon-black-loaded silicone composites have been fabricated for use as semisolid phantom materials. The electrical properties of various carbon loadings have been measured as a function of frequency (1000 Hz to 1 MHz) and compared to reported electrical properties of various biological tissues. Unavoidable clustering of the carbon black in the composite occurs, which leads to disordered suspension topologies in the resulting composite. Clustering or aggregation of metal particles in a dielectric host affect the electrical (both permittivity and conductivity) properties. These effects are generally not taken into account in classical predictive mixing rules for dielectrics. In addition, such cluster topologies lead to rapid, nonlinear increases of conductivity and permittivity of the phantom material as volume fractions of the carbon loading are increased. The conductor loading volume fraction, for which very rapid increases in permittivity and conductivity of the composite occur, is usually at the percolation-threshold close-packing limit $x = x_c = 0.63$ for random suspensions of spherical conductor particles. This is predicted by adapted Clausius-Mossotti and Maxwell-Garnett mixing rules that take into account the effects of clustering in the well- stirred but disordered conductor-particle suspensions.

The measured electrical properties of fabricated carbon-black-loaded silicone composites exhibit a threshold percolation at carbon loading fractions well below the close-packing limit expected in well stirred samples; e.g., at $x = x_c/3 = 0.21$. This is predicted by an adapted form of the classical Bruggeman rule reported here that takes into account the cluster topology of the carbon-black particles in the fabricated composites.

We have presented effective cluster models for two broad classes of permittivity and conductivity enhancements observed in low-frequency measurements on monodisperse suspensions of conductive spheres in a dielectric insulating host. The enhancements are attributed to higher multipole interactions in the carbon particle clusters. These multipole interactions also produce the particle aggregations. Nonpercolating suspensions are

treated as mixtures of isolated conductive (carbon) spheres and closed-packed conductive aggregates of spheres using the Clausius-Mossotti formulation, whereas percolating suspensions are treated as mixtures of randomly intermingled conductive and dielectric insulating regions using the symmetric Bruggeman formulation. In the cluster-adapted Bruggeman formulation, the conductive regions are close-packed with clusters of carbon spherical particles, while the dielectric regions contain only isolated spheres.

We observed that the only difference in conductivity and permittivity enhancement between the predictive models is the cluster topology. Any chemically inert conductor and insulator can be used as inclusion particle and host. In well-stirred samples, the permittivity increases rapidly but smoothly with carbon loading up to the close-packing limit; conductivity varies linearly up to the close-packing limit. The other type of suspension is more difficult to prepare reproducibly because such suspensions exhibit percolation and rapidly increasing conductivity and permittivity at volume fractions well-below the close-packing limit. For biologic phantom materials, carbon-black concentrations should be below the expected percolation threshold. Fabrication methods affecting the cluster topology of the incorporated carbon black that result in percolation thresholds near the close-packing limit need to be explored. In addition, the relation of percolation at thermodynamic equilibrium with differing annealing temperatures and annealing times needs to be studied. The type of cluster topology and percolation threshold behavior will be reflected in low-frequency electrical property measurements.

Conductivity measurements of carbon-black-filled silicone polymer composites from 10 °C to 25 °C exhibit a temperature behavior similar to that of an extrinsic, partially compensated n-type semiconductor. The measured conductivity-temperature dependence can be related to the conduction-band density of states, as well as donor and acceptor concentrations in the composite. The carrier density has a temperature dependence for a compensated semiconductor different from that of the carrier mobility, whose temperature dependence depends on the scattering mechanism. This complicates the conversion of σ vs. T into carrier density vs. T in predictive models of temperature dependence. A large positive temperature coefficient with respect to resistance was observed at temperatures greater than 40 °C for the 7 % carbon-black-filled silicone composite, consistent with nonpercolative behavior at these temperatures. For phantom biologic materials using carbon-black-loaded composites, temperatures should be kept below 40 °C to avoid unacceptable conductivity variations.

Financial support from the DOJ National Institute of Justice and the NIST-EEEL Office of Law Enforcement Standards is gratefully acknowledged.

Chapter 7

References

[1] Baker-Jarvis, J.; Kaiser, R.; Janezic, M.D.; Paulter, N.G.; Stricklett, K.L., "Metal Detector Studies: Research Materials," *Natl. Inst. Standards Techn. Technical Note 1514*, 2002.

[2] Gabriel, C.; Gestblom, B., "Microwave absorption in aqueous solutions," *Nature*, 328, pp. 145-146, 1987.

[3] Sihvola, A., *Electromagnetic Mixing Formulas and Applications*, IEE Electromagnetic Wave Series 47: Cornwall, U.K., 1999.

[4] Lorenz, L., "Experimentale og theoretiske Undersoegelser over Legemernes Brydningsforhold," *Det Kongelige Danske Videnskabernes Selskabs Skrifter*, Naturvidenskabelig og mathematisk afdeling, Femte Raekke, Ottonde Bind, 8, pp. 205-248, 1869.

[5] Lorenz, L., "Über die Refractionsconstante," *Annalen der Physik und Chemie*, IX, 9, pp. 70-103, 1880.

[6] Lorentz, H.A., "Über die Beziehung zwischen der Fortphflanzungsgeschwindigkeit des Lichtes und der Körperdichte," *Annalen der Physik und Chemie*, IX, 4, pp. 641-665, 1880.

[7] Bernal, J.D., "Geometry of the structure of monatomic liquids," *Nature*, 185, pp. 68-70, 1960.

[8] Coxeter, H.S.M., *Introduction to Geometry*, John Wiley: New York, 1962.

[9] Geyer, R.G.; Mantese J.; Baker-Jarvis, J.,"Effective medium theory for ferrite-loaded materials," *Natl. Inst. Standards Techn. Technical Note 1371*, 1994.

[10] Bruggeman, D.A.G., "Berechnung verschiedener physikalischer Konstanten von heterogenen Substanzen," *Ann. Phys. Leipzig*, 24, pp. 636-679, 1935.

[11] Lewin, L., "Electrical constants of spherical conducting particles in a dielectric," *J. IEE London*, 94, part III, pp. 65-68, 1947.

[12] Doyle, W.T., "Particle clustering and dielectric enhancement in percolating metal-insulator composites," *J. Appl. Phys.*, 78, pp. 6165-6169, 1995.

[13] Rayleigh, Lord, "On the influence of obstacles arranged in rectangular order upon the properties of the medium," *Philosophical Magazine*, pp. 481-502, **34**, 1892.

[14] Hartshorn, L.; Ward, W.H., "The measurement of the permittivity and power factor of dielectrics at frequencies 10^4 to 10^8 cycles per second," *J. Inst. Elec. Eng.*, 79, pp. 597-609, 1936.

[15] Von Hippel, A., *Dielectric Materials and Applications.* Cambridge, MA: M.I.T. Press, 1954.

[16] Somlo, P.I., "The discontinuity capacitance and the effective position of a shielded open circuit in a coaxial line," *Proc. Inst. Radio Elec. Eng. Australia*, 28, pp. 7-9, 1967.

[17] Bussey, H.E., "Dielectric measurements in a shielded open circuit coaxial line," *IEEE Trans. Instrum. Meas.*, IM-29, pp. 120-124, 1980.

[18] Stuchly, M.A.; Stuchly, S.S., "Coaxial line reflection methods for measuring dielectric properties of biologic substance at radio and microwave frequencies: A review," *IEEE Trans. Instrum. Meas.*, IM-29, pp. 176-183, 1980.

[19] Jesch, R.L., "Dielectric measurements of iol shales as functions of temperature and frequency," *IEEE Trans. Geosci. Remote Sensing*, GE-22, pp. 99-105, 1984.

[20] Scott, W.R.; Smith, G.S., "Error analysis for dielectric spectroscopy using shielded open-circuited coaxial lines of general length," *IEEE Trans. Instrum. Meas.*, IM-35, pp. 130-137, 1986.

[21] Jenkins, S.; Hodgetts, T.E.; Clarke, R.N.; Preece, A.W., "Dielectric measure-

ments on reference liquids using automatic network analyzers and calculable geometries," *Meas. Sci. Tech.*, 1, pp. 691-702, 1990.

[22] Baker-Jarvis, J.; Janezic, M.D.; Jones, C.A., "Shielded open- circuited sample holder for dielectric measurements of solids and liquids," *IEEE Trans. Instrum. Meas.*, 47, pp. 338-344, 1998.

[23] Wu, G.; Asai, S.; Zhang, C.; Miura, T.; Sumita, M., "A delay of percolation time in carbon-black-filled conductive polymer composites," *J. Appl. Phys.*, 88, pp. 1480-1487, 2000.

[24] Geyer, R.G., "Dielectric characterization and reference materials," *Natl. Inst. Stand. Technol. Technical Note 1338*, 1990.

[25] Baker-Jarvis, J.; Grosvenor, J.H., "Dielectric and magnetic measurements from −50 °C to 200 °C and in the frequency band 50 MHz to 2 GHz," NISTIR 5045, Natl. Inst. Stand. Technol., 1996.

[26] Kittel, C., *Thermal Physics*, John Wiley & Sons, Inc., New York, N.Y., 1969.

[27] Sachs, M., *Solid State Theory*, McGraw-Hill, New York, N.Y., 1963.

[28] Carmona, F.; Ravier, J., "Electrical properties and mesostructure of carbon black-filled polymers," *Carbon*, 40, pp. 151-156, 2002.

*U.S. GPO 2003-0-573-018/40221

NIST Technical Publications

Periodical

Journal of Research of the National Institute of Standards and Technology—Reports NIST research and development in metrology and related fields of physical science, engineering, applied mathematics, statistics, biotechnology, and information technology. Papers cover a broad range of subjects, with major emphasis on measurement methodology and the basic technology underlying standardization. Also included from time to time are survey articles on topics closely related to the Institute's technical and scientific programs. Issued six times a year.

Nonperiodicals

Monographs—Major contributions to the technical literature on various subjects related to the Institute's scientific and technical activities.

Handbooks—Recommended codes of engineering and industrial practice (including safety codes) developed in cooperation with interested industries, professional organizations, and regulatory bodies.

Special Publications—Include proceedings of conferences sponsored by NIST, NIST annual reports, and other special publications appropriate to this grouping such as wall charts, pocket cards, and bibliographies.

National Standard Reference Data Series—Provides quantitative data on the physical and chemical properties of materials, compiled from the world's literature and critically evaluated. Developed under a worldwide program coordinated by NIST under the authority of the National Standard Data Act (Public Law 90-396). NOTE: The Journal of Physical and Chemical Reference Data (JPCRD) is published bimonthly for NIST by the American Institute of Physics (AIP). Subscription orders and renewals are available from AIP, P.O. Box 503284, St. Louis, MO 63150-3284.

Building Science Series—Disseminates technical information developed at the Institute on building materials, components, systems, and whole structures. The series presents research results, test methods, and performance criteria related to the structural and environmental functions and the durability and safety characteristics of building elements and systems.

Technical Notes—Studies or reports which are complete in themselves but restrictive in their treatment of a subject. Analogous to monographs but not so comprehensive in scope or definitive in treatment of the subject area. Often serve as a vehicle for final reports of work performed at NIST under the sponsorship of other government agencies.

Voluntary Product Standards—Developed under procedures published by the Department of Commerce in Part 10, Title 15, of the Code of Federal Regulations. The standards establish nationally recognized requirements for products, and provide all concerned interests with a basis for common understanding of the characteristics of the products. NIST administers this program in support of the efforts of private-sector standardizing organizations.

Order the **following** *NIST publications—FIPS and NISTIRs—from the National Technical Information Service, Springfield, VA 22161.*

Federal Information Processing Standards Publications (FIPS PUB)—Publications in this series collectively constitute the Federal Information Processing Standards Register. The Register serves as the official source of information in the Federal Government regarding standards issued by NIST pursuant to the Federal Property and Administrative Services Act of 1949 as amended, Public Law 89-306 (79 Stat. 1127), and as implemented by Executive Order 11717 (38 FR 12315, dated May 11, 1973) and Part 6 of Title 15 CFR (Code of Federal Regulations).

NIST Interagency or Internal Reports (NISTIR)—The series includes interim or final reports on work performed by NIST for outside sponsors (both government and nongovernment). In general, initial distribution is handled by the sponsor; public distribution is handled by sales through the National Technical Information Service, Springfield, VA 22161, in hard copy, electronic media, or microfiche form. NISTIR's may also report results of NIST projects of transitory or limited interest, including those that will be published subsequently in more comprehensive form.

U.S. Department of Commerce
National Institute of Standards and Technology
325 Broadway
Boulder, Colorado 80305-3328

Official Business
Penalty for Private Use, $300